

## Supporting Information

# Construction of Heterostructure Based on Hierarchical Bi<sub>2</sub>MoO<sub>6</sub> and G-C<sub>3</sub>N<sub>4</sub> with Ease for Impressive Performance in Photoelectrocatalytic Water Splitting and Supercapacitor

C. Murugan,<sup>a,b</sup> M. Karnan,<sup>a,b</sup> M. Sathish<sup>a,b</sup> and A. Pandikumar<sup>a,b\*</sup>

<sup>a</sup>Functional Materials Division, CSIR-Central Electrochemical Research Institute, Karaikudi-630 003, Tamil Nadu, India.

<sup>b</sup>Academy of Scientific and Innovative Research (AcSIR), Ghaziabad- 201002, India

\*Corresponding Author E-mail: [pandikumarinbox@gmail.com](mailto:pandikumarinbox@gmail.com); [pandikumar@ceceri.res.in](mailto:pandikumar@ceceri.res.in)

### Characterization techniques

The diffuse reflectance spectra of the as prepared nanohybrid materials were recorded using BaSO<sub>4</sub> as a reference in a Varian UV–Visible spectrophotometer (Model: Cary 500 Scan) equipped with a diffuse reflectance accessory. The phase purity and crystalline nature of the samples were analysed by recording X–ray diffraction using a Bruker AXS D8 Advance X-ray diffractometer with Cu K $\alpha$  radiation ( $\lambda = 1.54178 \text{ \AA}$ ). The FT-IR spectra were recorded using Bruker Optik GmbH, Germany (Model: TENSOR 27) Fourier-transform infrared spectrophotometer. The chemical nature of the samples was studied using X-ray photoelectron spectroscopy (XPS) with Mg K $\alpha$  (1253.6 eV) as X-ray source (Thermo Scientific, MULTILAB 2000). The size and surface morphology were characterized using Carl Zeiss AG (Supra 55VP) field emission scanning electron microscopy with an acceleration voltage of 30kV fitted with EDAX and elemental mapping accessory. The STEM and elemental mapping were performed in HAADF mode. The surface area of the materials was measured using surface area and pore size analyzer (Quantachrome, NOVA 3200e). The wettability study was carried out using contact angle measurement by VCA optima (S/N. 1020041134), 5  $\mu$ L drops of water were

sequentially deposited on surface of the electrode material (prepared material: super-P carbon: PVDF in the weight ratio of 75:20:5) coated on flexible graphite paper.

### **Photoelectrochemical measurements**

Photoelectrochemical experiments were carried out using a three-electrode system with an electrochemical workstation (BioLogic SP-150) using 1 M KOH (pH = 13.22) as an electrolyte. The counter electrode is platinum wire, reference electrode is mercury-mercury oxide (Hg/HgO) and working electrode is the prepared materials coated film. When the 5 mg of prepared sample and 1 mg of polyvinylidene fluoride (PVDF) were mixed in a mortar and then 25  $\mu$ L of NNP (N-Phenethyl-4-piperidone) was added and mixed in a mortar, a concentrated paste was formed. The paste was coated in an FTO (Fluorine doped Tin Oxide) glass by doctor blade method. The prepared electrode was allowed to dry at 80 °C overnight. The ORIEL LCS-100 solar simulator (Newport, USA) with AM 1.5G (100 mW cm<sup>-2</sup>) filter was employed as light source. The photocurrent response and electrochemical impedance spectroscopy (EIS) were measured at room temperature. All of the measured potentials were converted with respect to the reversible hydrogen electrode (RHE) using eqn. (S1) with measured pH of electrolyte.

$$E_{RHE} = E_{Hg/HgO} + 0.0591 \times pH + E_{Hg/HgO}^{\circ} \quad (S1)$$

Where,  $E_{RHE}$  is the converted potential vs. RHE,  $E_{Hg/HgO}^{\circ} = 0.098$  V at 25 °C, pH and  $E_{Hg/HgO}$  is the experimentally measured potential against Hg/HgO reference.<sup>1</sup>

### **Electrochemical characterization**

For the electrochemical studies, the working electrode was contrived by mixing gCN/BMO nanohybrid materials (active material), super-P carbon (conducting carbon) and

polyvinylidene fluoride (PVDF, binder) in the weight ratio of 75:20:5, respectively and grinded well using agate mortar and pestle to obtain fine mixer. The electrode mixer was then dispersed using N-Methyl-2-pyrrolidone (NMP) solvent to make slurry and coated over flexible graphite paper substrate (2 x 2 cm<sup>2</sup>). The electrode materials coated flexible graphite paper was placed in vacuum oven at 80 °C for overnight drying and the electrode material loading was optimized to ~2 mg/cm<sup>2</sup>. The gCN/BMO coated graphite paper, a slice of Pt foil and Hg/HgO (20% KOH) was used as a working, counter and reference electrode, respectively. The electrode material of bare BMO and gCN were also prepared identically for the comparison purpose. The electrochemical property of gCN/BMO nanohybrid materials was characterized by CV, CD and EIS analysis using 3.5 M KOH (20% KOH) as electrolyte. The CV and CD experiments were carried out in the potential range of -1.2 to 0.6 V (vs. Hg/HgO) for bare BMO and gCN/BMO nanohybrid materials at different scan rates and current densities, respectively. Similarly, bare gCN was also studied in the potential range of 0 to 0.6 V (vs. Hg/HgO). From the discharge profile, the specific capacitance (for non-faradaic materials) and specific capacity (for faradaic materials) of the electrode was calculated using the eqn. (S2) and (S3).<sup>2</sup>

$$C_{sp} = \frac{I \Delta t}{m \Delta V} \quad (S2)$$

$$Q_{sp} = \frac{I \Delta t}{m} \quad (S3)$$

Where  $C_{sp}$  (F g<sup>-1</sup>) is the specific capacitance of the electrode materials,  $Q_{sp}$  (C g<sup>-1</sup>) is the specific capacity of the electrode materials,  $I$  (A) is the applied charge/discharge current,  $\Delta t$  (sec) is the discharge time and  $m$  (g) is the active mass of the electrode materials and  $\Delta V$  (V) is working potential.

Also, the symmetric full cell was fabricated using best nanohybrid electrode material (5-gCN/BMO) from the half-cell measurement. The specific capacity ( $Q_{sp}$ ), coulombic efficiency ( $\eta$ ), energy density (E) and power density (P) of the fabricated symmetric supercapacitor device was calculated from the eqn. (S4 to 8).<sup>3-5</sup>

$$Q_t = \frac{I \Delta t}{M} \quad (S4)$$

$$Q_{sp} = 4Q_t \quad (S5)$$

$$\eta = \frac{\Delta t_{discharge}}{\Delta t_{charge}} \times 100\% \quad (S6)$$

$$E = \frac{1}{2} Q_t V \quad (S7)$$

$$P = \frac{E}{\Delta t} \quad (S8)$$

Here,  $Q_{sp}$  is the specific capacity ( $C g^{-1}$ ), I is the charge-discharge current (A),  $\Delta t$  is the total discharge time (sec), M is the total active mass of the electrode materials (g) and  $\Delta V$  is potential window (V). EIS experiments were performed with bias of 5 mV in the frequency range of 10 mHz to 100 kHz and the data was analyzed using a Nyquist plot.

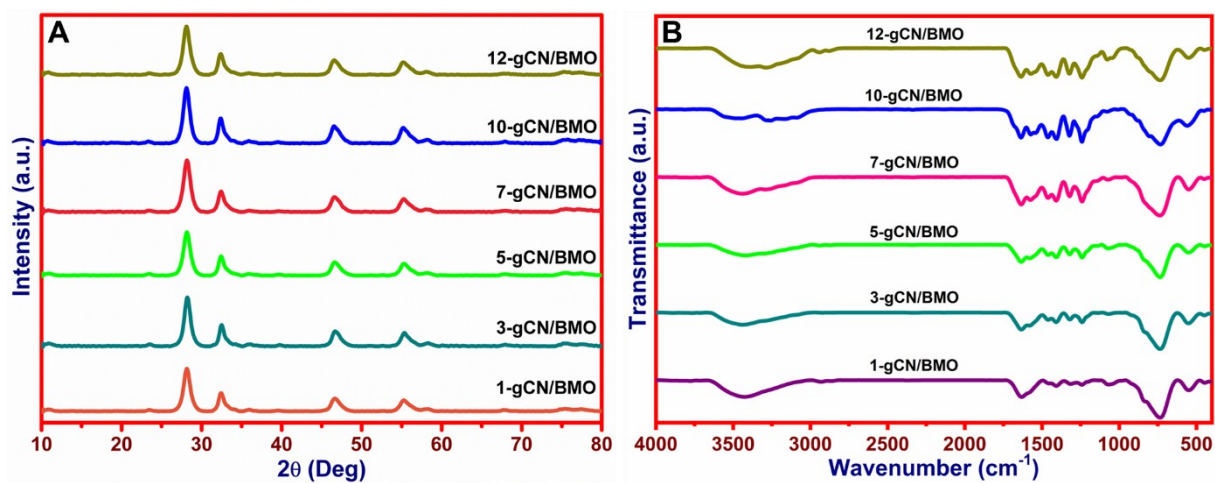


Figure S1. (A) XRD patterns and (B) FTIR spectra of gCN/BMO with different wt. % of gCN.

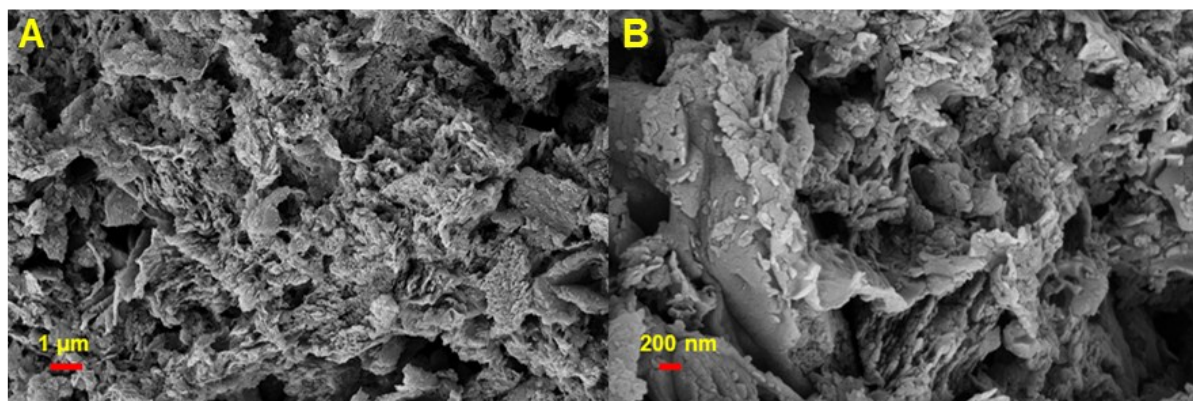


Figure S2. (A) & (B) are FESEM images of pristine-gCN.

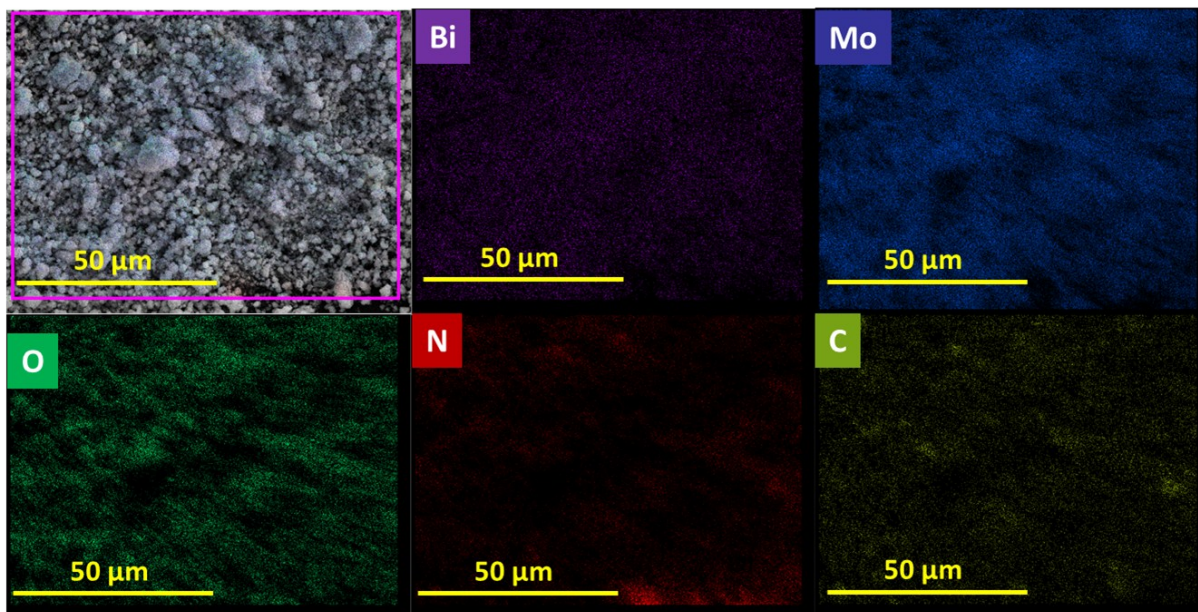


Figure S3. FESEM image of gCN/BMO nanohybrid material and their corresponding elemental mapping.

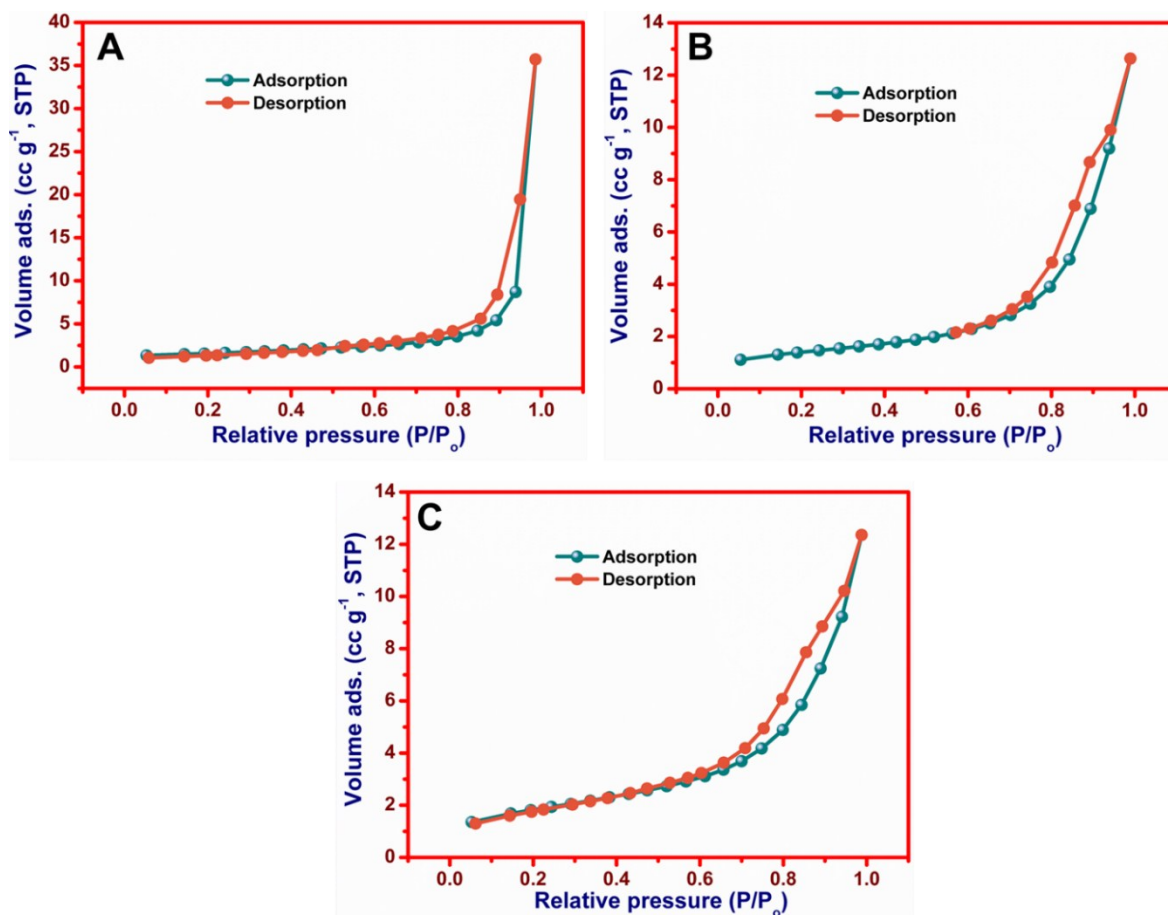


Figure S4. Nitrogen adsorption-desorption isotherms obtained for (A) gCN, (B) BMO and (C) 5-gCN/BMO.

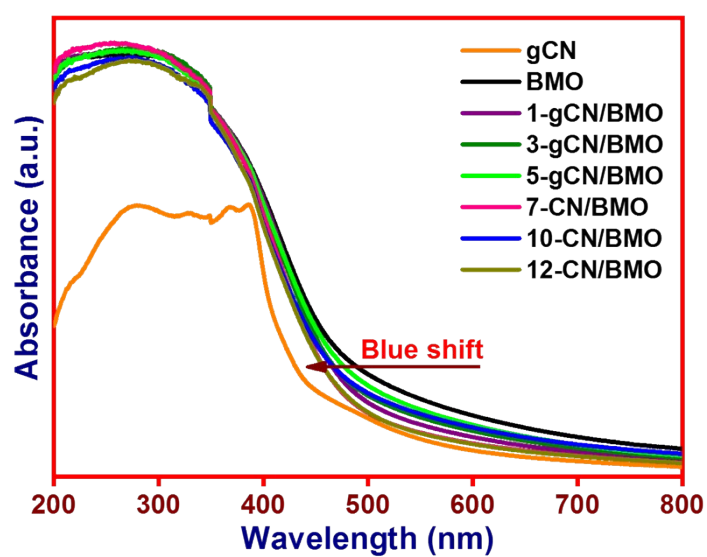


Figure S5. UV-Vis absorption spectra obtained for gCN, BMO and gCN/BMO with different wt. % of gCN.

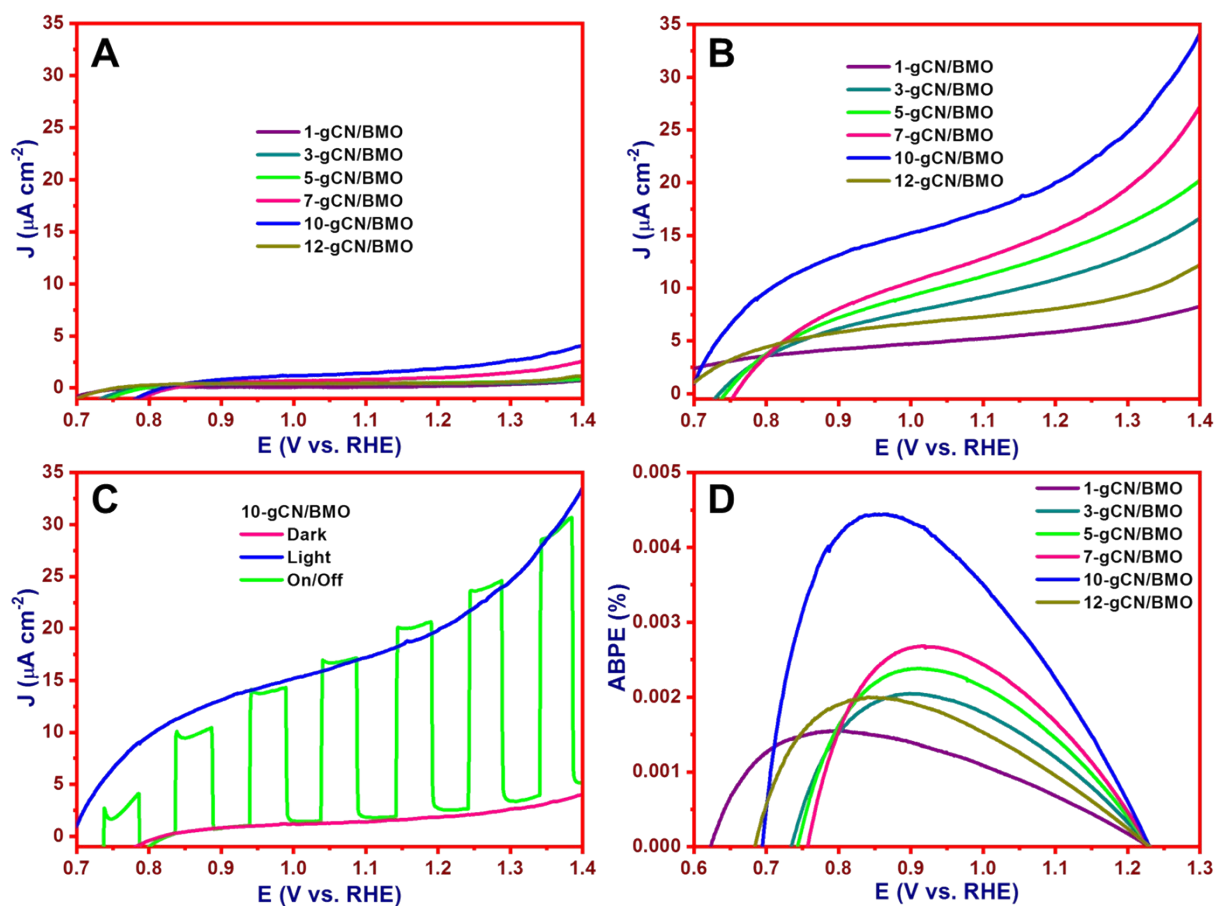


Figure S6. (A) Linear sweep voltammograms obtained gCN/BMO with different wt. % of gCN under the dark at a scan rate of 10 mV/s in 1 M KOH; (B) Linear sweep voltammograms obtained gCN/BMO with different wt. % of gCN under the simulated solar illumination of 100  $\text{mW cm}^{-2}$  (AM 1.5G) at a scan rate of 10 mV/s in 1 M KOH; (C) Linear sweep voltammograms obtained for 10-gCN/BMO under dark, light and chopped condition. (D) Plot of ABPE (%) vs. applied potential obtained for gCN/BMO with different wt. % of gCN.

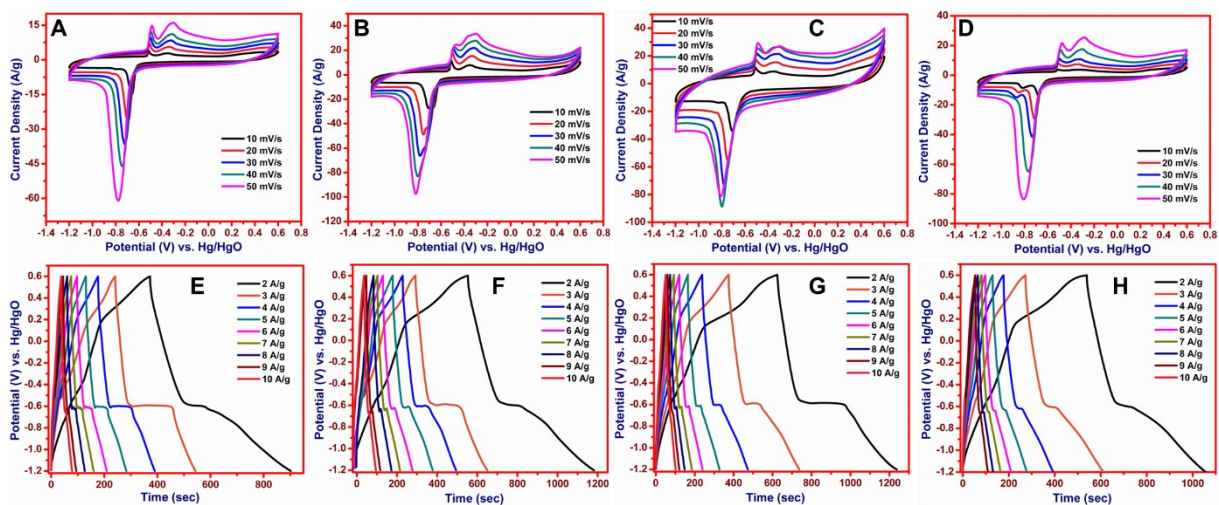


Figure S7. CV profiles of (A) 1-gCN/BMO, (B) 3-gCN/BMO, (C) 7-gCN/BMO and (D) 10-gCN/BMO nanohybrid electrode materials at different scan rates, respectively; CD profile of (E) 1-gCN/BMO, (F) 3-gCN/BMO, (G) 7-gCN/BMO and (H) 10-gCN/BMO nanohybrid electrode materials at different current densities.

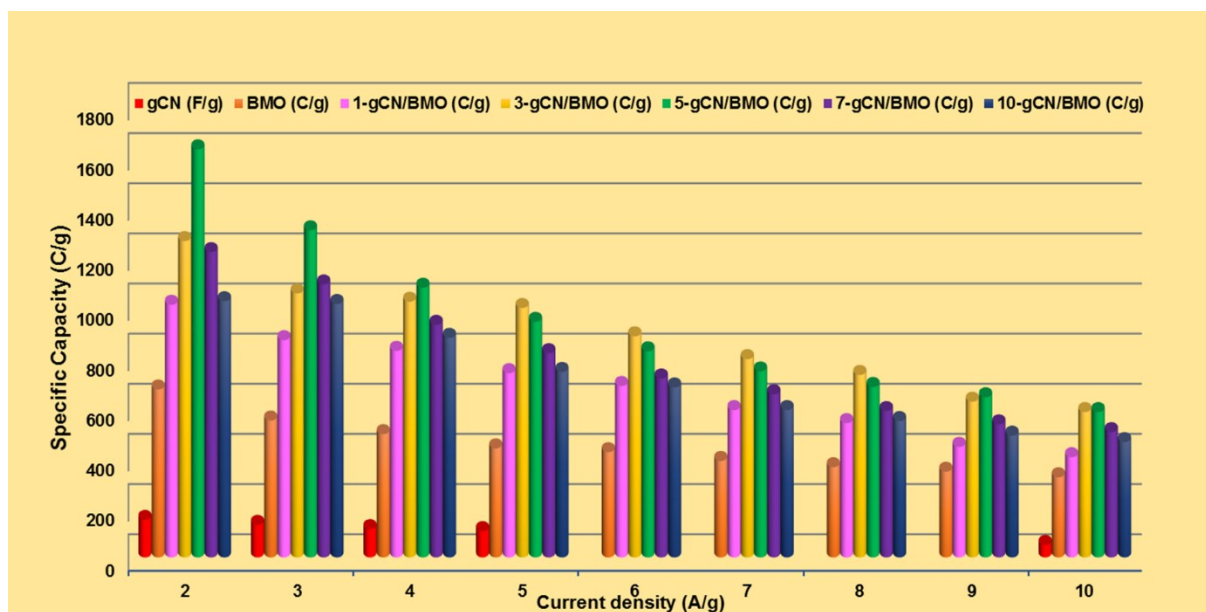


Figure S8. Specific capacity of the gCN, BMO and gCN/BMO with different wt. % of gCN as a function of the different current density.

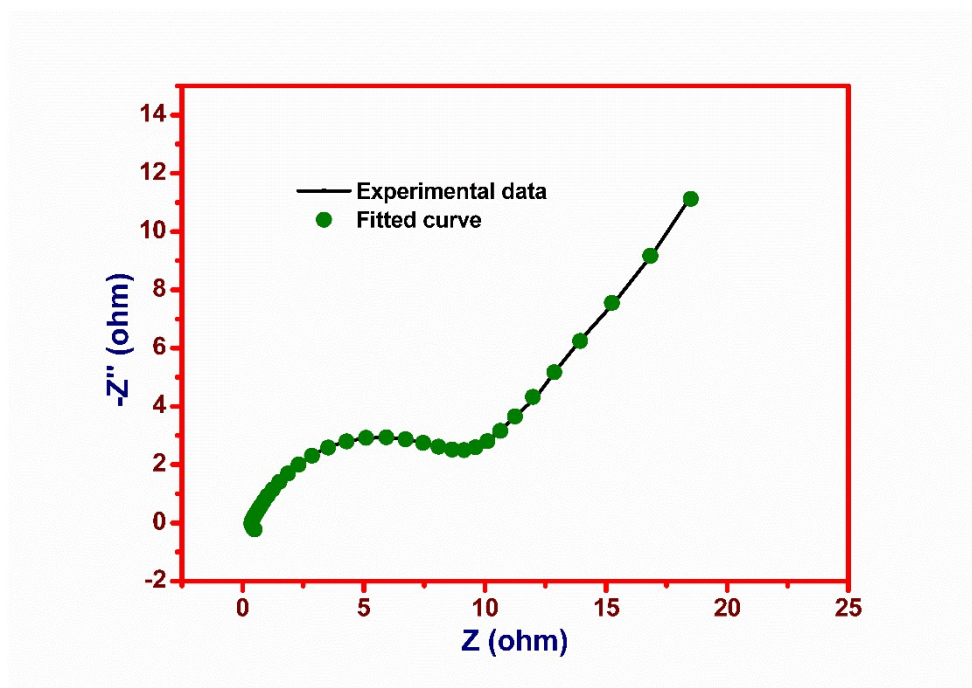


Figure S9. Nyquist plot obtained for the fabricated symmetric cell based on 5-gCN/BMO.

## Reference

- 1 X. Han, Y. Wei, J. Su and Y. Zhao, *ACS Sustain. Chem. Eng.*, 2018, **6**, 14695–14703.
- 2 K. Subramani, D. Jeyakumar and M. Sathish, *Phys. Chem. Chem. Phys.*, 2014, **16**, 4952–4961.
- 3 S. Kaipannan and S. Marappan, *Sci. Rep.*, 2019, **9**, 1104.
- 4 K. Subramani, N. Sudhan, M. Karnan and M. Sathish, *ChemistrySelect*, 2017, **2**, 11384–11392.
- 5 Y. Cui, J. Zhang, C. Jin, Y. Liu, W. Luo and W. Zheng, *Small*, 2018, **15**, 1804318.